High-efficiency half-Heusler thermoelectric modules enabled by self-propagating synthesis and topologic structure optimization

Yunfei Xing, [ab] Ruiheng Liu ,*[ab] Jinchen Liao, [a] Qihao Zhang, [a] Xugui Xia, [a] Chao Wang, [a] Hui Huang, [ab] Jing Chu, [ab] Ming Gu, [a] Tiejun Zhu, [c] Chenxi Zhu,[a] Fangfang Xu,[a] Dongxu Yao, [a] Yuping Zeng, [a] Shengqiang Bai, *[ab] Ctirad Uher, [d] and Lidong Chen [ab]

[a] The State Key Laboratory of High Performance Ceramics and Superfine Microstructure, Shanghai Institute of Ceramics, Chinese Academy of Sciences, Shanghai 20050, China.

[b] Center of Materials Science and Optoelectronics Engineering, University of Chinese Academy of Sciences, Beijing 100049, China.

[c] State Key Laboratory of Silicon Materials and School of Materials Science and Engineering, Zhejiang University, Hangzhou 310027, China.

[d] Department of Physics, University of Michigan, Ann Arbor, MI 48109, USA.

Formation energy calculation of alloyed HH compounds

Formation enthalpies (ΔH) of HH alloys were obtained by density functional theory (DFT) calculations at T = 0 K. 4×2×2 supercells of special quasirandom structure (SQS)[1] generated by using the Monte Carlo SQS tool implemented in Alloy Theoretical Automated Toolkit (ATAT) were used for calculation. DFT calculations were performed using the Vienna Ab Initio Simulation Package (VASP) implemented with the projector-augmented wave (PAW) potentials and a plane-wave basis set.

The generalized gradient approximation of Perdew, Burke and Ernzerhof (PBE) was chosen for the exchange-correlation functional. A 5×10×10 Monkhorst-Pack k-point mesh was used to sample the Brillouin zone and the kinetic energy cutoff of 400 eV was used for the plane-wave basis set. The energy convergence criterion for the self-consistent calculation was set to 10^{-6} eV.

Table S1. Formation enthalpy (ΔH) and barrier energy (E_b) for ZrNiSn and ZrCoSb-based HH alloys

Compounds	ΔH (kJmol^{-1})	E_b (kJmol^{-1})
ZrNiSn	**-209.7**	**38.8**
$Zr_{0.75}Hf_{0.25}NiSn$	**-201.5**	**-**
$Zr_{0.5}Hf_{0.5}NiSn$	**-195.9**	**42.6**
$Zr_{0.25}Hf_{0.75}NiSn$	**-190.3**	**-**
$Zr_{0.5}Hf_{0.5}NiSn_{0.75}Sb_{0.25}$	**-193.7**	**-**
$Zr_{0.5}Hf_{0.5}NiSn_{0.5}Sb_{0.5}$	**-186.9**	
$Zr_{0.5}Hf_{0.5}NiSn_{0.25}Sb_{0.75}$	**-177.3**	
HfNiSn	**-187.6**	**40.1**
ZrCoSb	**-227.0**	**30.7**
$Zr_{0.75}Hf_{0.75}CoSb$	**-221.5**	**-**
$Zr_{0.5}Hf_{0.5}CoSb$	**-215.9**	**40.1**
$Zr_{0.25}Hf_{0.75}CoSb$	**-210.2**	**-**
$Zr_{0.5}Hf_{0.5}CoSb_{0.75}Sn_{0.25}$	**-190.4**	**-**
$Zr_{0.5}Hf_{0.5}CoSb_{0.5}Sn_{0.5}$	**-166.0**	
HfCoSb	**-205.4**	**37.7**

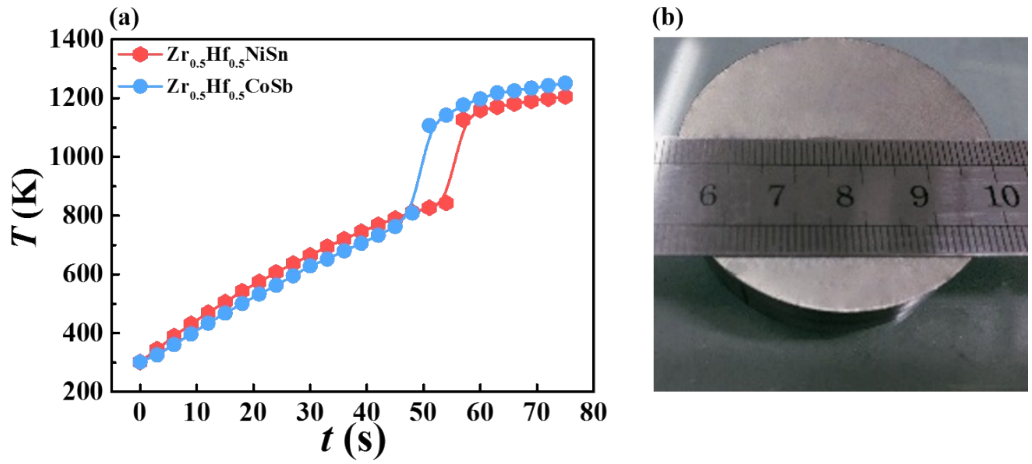

Figure S1: (a) Ignition point of $Zr_{0.5}Hf_{0.5}NiSn$ and $Zr_{0.5}Hf_{0.5}CoSb$. (b) The pressed 200g pellet for SHS.

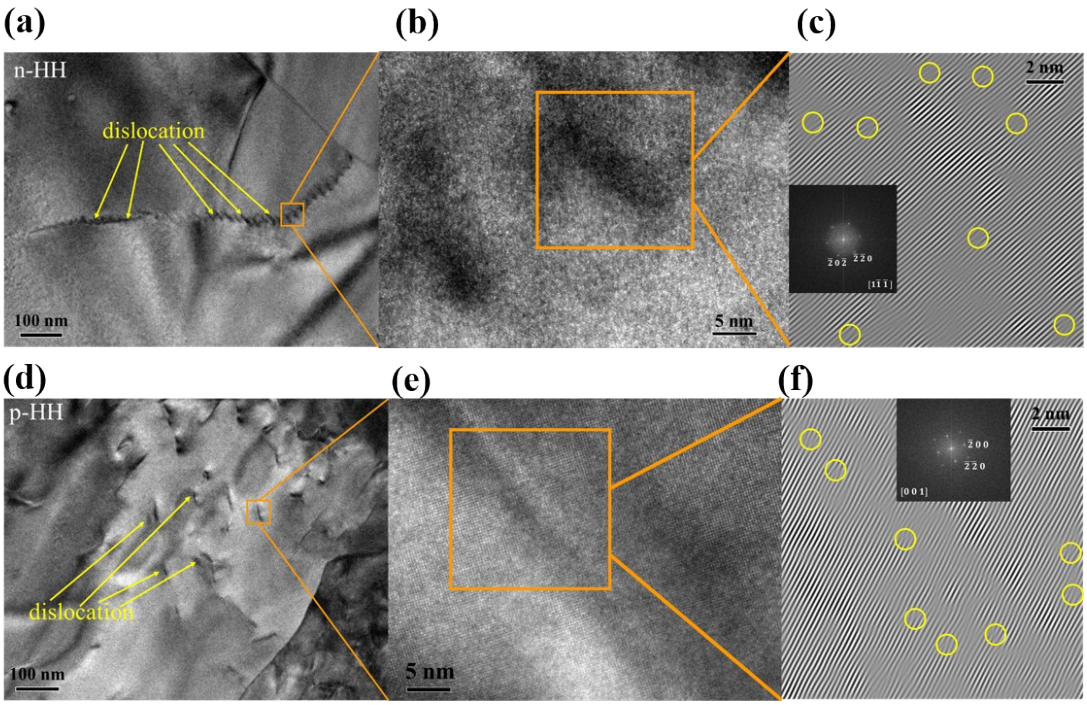

Figure S2: (a) Low-magnification TEM image of SHS-prepared $Zr_{0.5}Hf_{0.5}NiSn_{0.985}Sb_{0.015}$. (b) Enlarged view of the boxed region in (a). (c) Inverse FFT image of (b). (d) Low-magnification TEM image of SHS-prepared $Zr_{0.5}Hf_{0.5}CoSb_{0.8}Sn_{0.2}$. (e) Enlarged view of the boxed region in (d). (f) Inverse FFT image of (e).

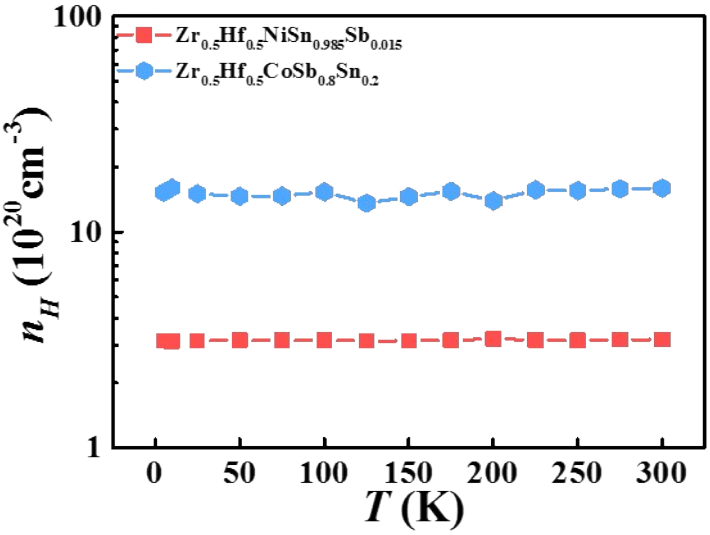

Figure S3: Hall carrier concentration as a function of temperature.

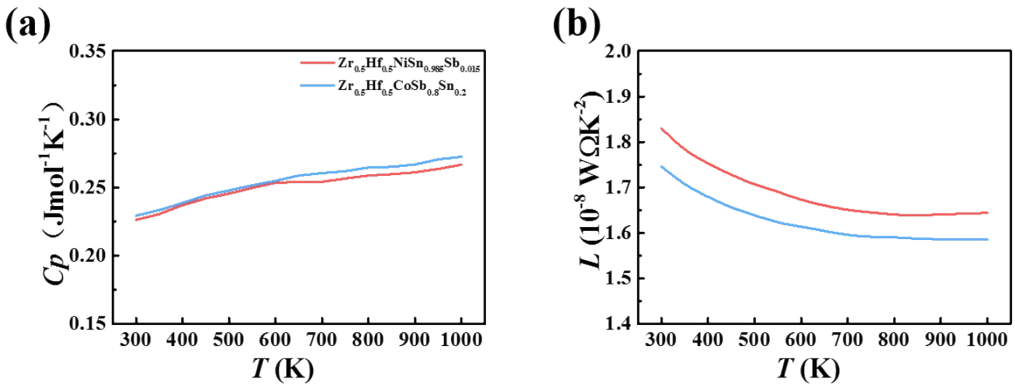

Figure S4: (a) The temperature-dependent specific heat. (b) The Lorenz number obtained from the reduced Fermi energy.

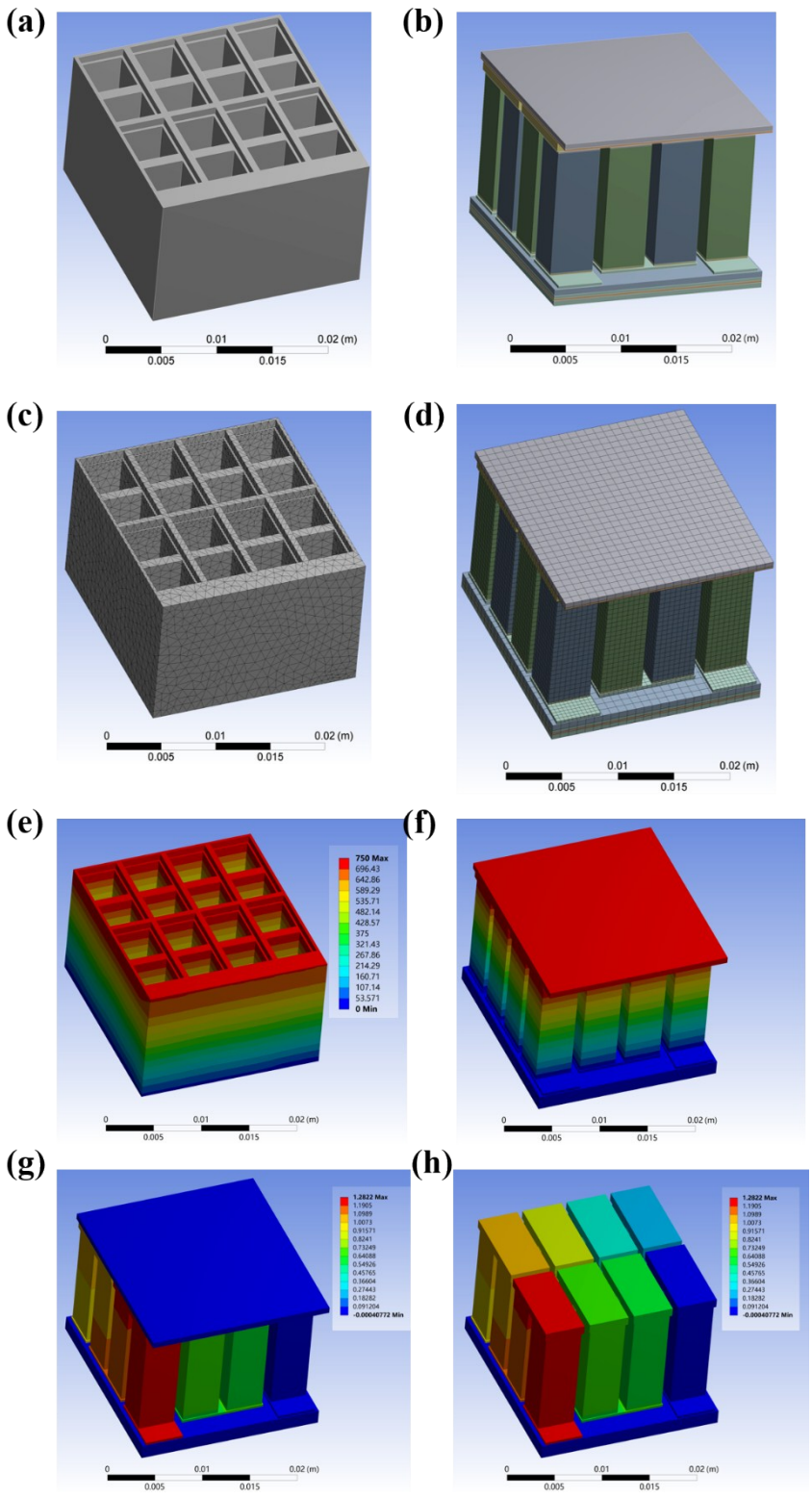

Figure S5: (a) Fillers appearance. (b) Image of an 8-pairs module. (c) Meshing result of the fillers. (d) Meshing result of the module. (e) Temperature distribution of fillers; (f) Temperature distribution of the module. (g) Electrical voltage distribution along the module. (f) Electrical voltage distribution inside of the single module.

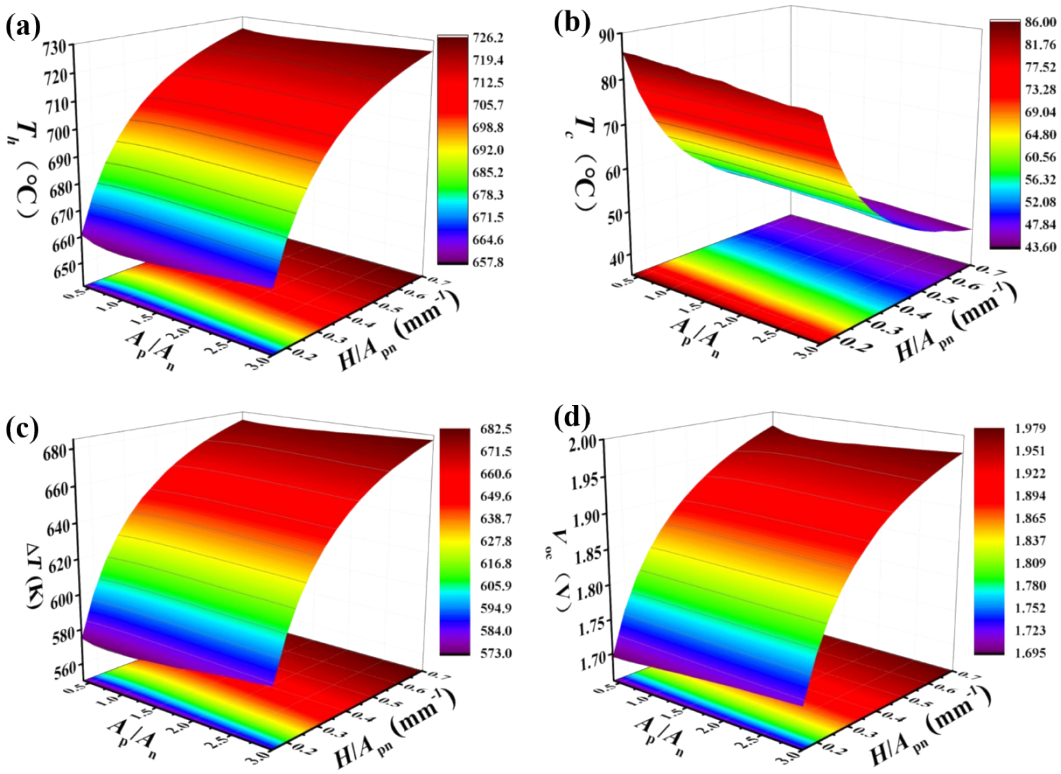

Figure S6: 3D plots relating (a) hot-side temperature (T_h); (b) cold-side temperature (T_c); (c) effective temperature difference; and (d) the open circuit voltage.

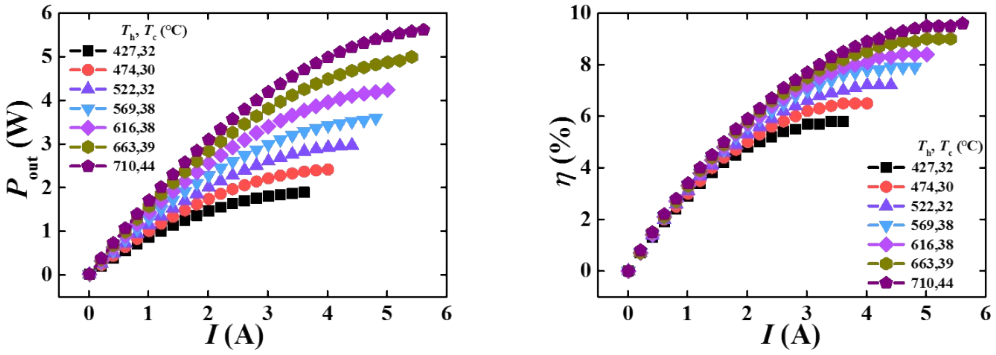

Figure S7: (a) The output power of the HH single-stage module as a function of the current under different operating temperatures. (b) Conversion efficiency of the module with A_p/A_n=1.65 and H/A_{pn}=0.47 as a function of the current under different operating temperatures.

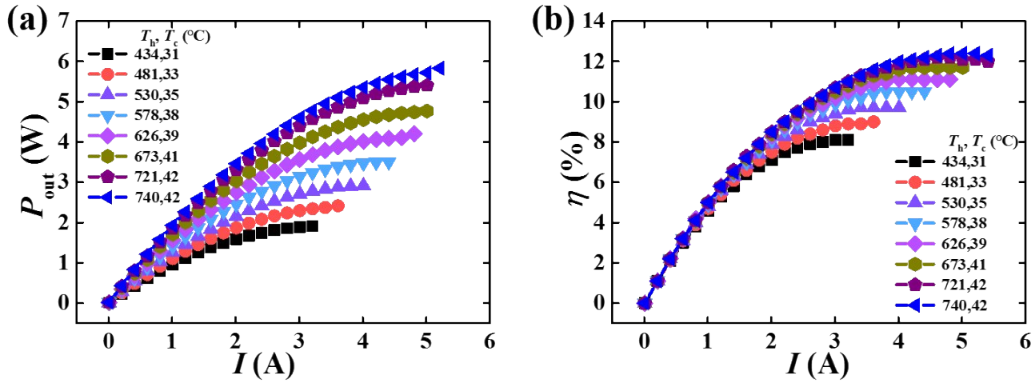

Figure S8: (a) The output power of the HH-BT segmented module as a function of the current under different operating temperatures. (b) Conversion efficiency of the segmented module as a function of the current under different operating temperatures.

The long-time stability experiment was conducted at T_{heater}=973 K and T_{cooler}=303 K and the thermal-cycle experiment kept the T_{cooler}=303 K, the T_{heater} was shocked between 973 K and 773 K and each cycle is about 45 minutes.

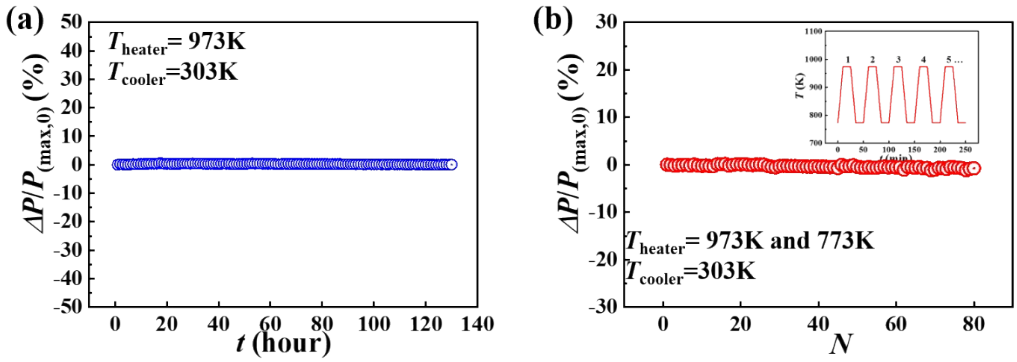

Figure S9. (a) The result of (a) aging testing on the HH single-stage module under the constant temperature difference of 670 K under T_{heater}=973 K and T_{cooler}=303 K. (b) thermal cycle testing on the single-stage module.

[1] van de Walle, A., et al., Efficient stochastic generation of special quasirandom structures. Calphad-Computer Coupling of Phase Diagrams and Thermochemistry, 2013. 42: p. 13-18.